Boletín Médico del
Hospital Infantil de México

PERMANYER

Check for updates

PATHOLOGICAL CLINICAL CASE

Clinicopathological correlation of neonatal lung ultrasound. A pictorial essay

Daniel Ibarra-Ríos[1,2], Carlos A. Serrano Bello[3], Deneb A. Morales-Barquet[4], Talía Estrada-Rojas[5], Alejandra Sánchez-Cruz[6], Lourdes Ma. del C. Jamaica-Balderas[7], Sergio A. Patrón-Chi[8], and Horacio Márquez-González[2]*

[1]Expresidente, Asociación de Neonatólogos de la Ciudad y Valle de México; [2]Servicio de Investigación Clínica, Hospital Infantil de México Federico Gómez; [3]Departamento de Patología, Hospital Infantil de México Federico Gómez; [4]Departamento de Neonatología, Instituto Nacional de Perinatología Isidro Espinosa de los Reyes; [5]Responsable del Bioterio, Instituto Nacional de Perinatología Isidro Espinosa de los Reyes; [6]Departamento de Neonatología, Unidad Médica de Alta Especialidad, Hospital de Gineco Obstetricia No. 4, Luis Castelazo Ayala; [7]Departamento de Neumología, Hospital Infantil de México Federico Gómez; [8]Adscrito a Imagen Cardiovascular, Hospital Infantil de México Federico Gómez. Ciudad de México, México

Abstract

Lung ultrasound has become a valuable tool in neonatal intensive care practice, with exponential diffusion of evidence of its diagnostic and functional applications over the last decade. In this pictorial essay, we review animal models and clinical cases where diagnosis was confirmed with high-resolution pulmonary computed tomography/cardiac angiotomography, biopsies, or autopsies, pointing out the main ultrasound features of neonatal respiratory disorders.

Keywords: *Lung ultrasound. Newborn. Anatomic pathology. Animal model. Ultrasound. Computed axial tomography.*

Correlación clinicopatológica del ultrasonido pulmonar neonatal. Un ensayo gráfico

Resumen

El ultrasonido pulmonar se ha convertido en una herramienta valiosa en la práctica de cuidados intensivos neonatales, con una difusión exponencial de la evidencia sobre sus aplicaciones diagnósticas y funcionales durante la última década. En este ensayo gráfico revisamos modelos animales y casos clínicos en los cuales el diagnóstico se confirmó con tomografía computarizada pulmonar de alta resolución/angiotomografía cardiaca, biopsias o autopsias, señalando las principales características ecográficas de los trastornos respiratorios neonatales.

Palabras clave: *Ultrasonido pulmonar. Recién nacido. Anatomía patológica. Modelo animal. Ultrasonido. Tomografía axial computarizada.*

Correspondence:
Daniel Ibarra-Ríos
E-mail: ibarraneonato@gmail.com

Date of reception: 22-07-2025
Date of acceptance: 15-08-2025
DOI: 10.24875/BMHIM.25000085

Available online: 05-12-2025
Bol Med Hosp Infant Mex. 2025;82(Supl 5):38-53
www.bmhim.com

Introduction

Lung ultrasound (LU) has been increasingly used by emergency physicians, cardiologists, pneumologists, anesthesiologists, and intensivists to obtain anatomical and functional images at the patient's bedside. It has become a valuable tool in neonatal intensive care practice, with exponential diffusion of evidence of its diagnostic and functional applications over the last decade[1]. In this pictorial essay, we review animal models[2] and clinical cases where diagnosis was confirmed with high-resolution pulmonary computed tomography/cardiac angiotomography, biopsies, or autopsies, pointing out the main ultrasound features of neonatal respiratory disorders. Cases are grouped, reviewing the basic semiology of LU interpretation.

Normal LU

The bat sign is used to identify an intercostal space, the edge of the ribs being the wings and the pleural line the head. The pleural line is normally a smooth, regular, straight hyperechoic line under the ribs in newborns normally measuring less than 1 mm. Pleural sliding is normally seen as a horizontal to-and-fro motion of the pleural line, synchronized with respiratory movement. Its absence is always pathological. In M-mode, the seashore sign is observed (secondary to pleural sliding, generating a sandy image). A-lines are horizontal artifacts equidistant to the pleural line, appreciated during the insonation of an aerated lung[3] (Fig. 1).

B-Lines

Signifying an air/liquid interface, B-lines appear as laser-like vertical hyperechoic reverberation artifacts that arise from the pleural line, move synchronously with pleural sliding, and extend to the bottom of the screen without fading (Fig. 2). The presence of three or more well-spaced B-lines is defined as an interstitial syndrome and is pathologic representing interstitial edema. During transition, B-lines are used to diagnose respiratory distress syndrome (RDS), where B-lines can coalesce making A-lines disappear giving a white lung appearance (signifying interstitial and alveolar edema, fig. 3), and transient tachypnea of the newborn (TTN), where spared well aeriated areas are seen. Pleural line in RDS appears thick and irregular with collapse bronchogram, and in TTN a regular pleural line with no consolidation is a consistent finding[3]. After transition, B-lines are seen in

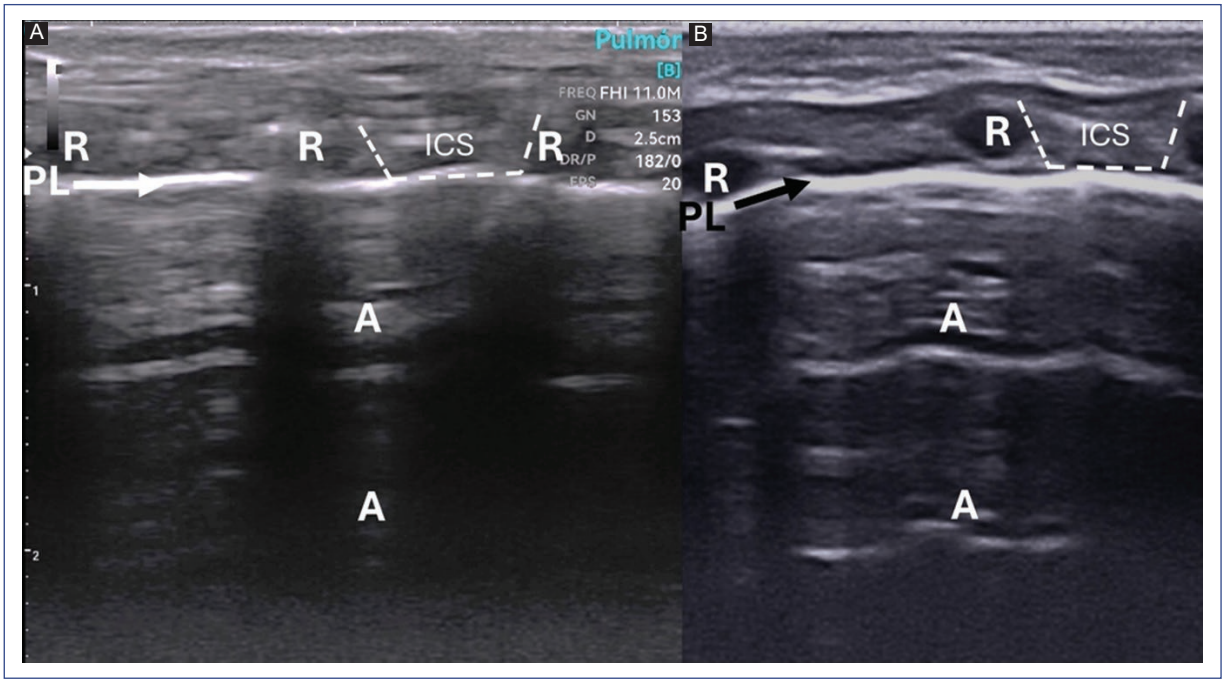

Figure 1. Normal longitudinal lung ultrasound in a human newborn and in an animal model. **A:** bio model for teaching: male Wistar rat weighing 800 g. Intramuscular sedation and analgesia were provided with tiletamine, zolazepam, and meloxicam. Note the bat sign between ribs (dashed line), the pleural line, and the A-lines. **B:** normal neonatal lung ultrasound. R: rib, ICS: intercostal space.

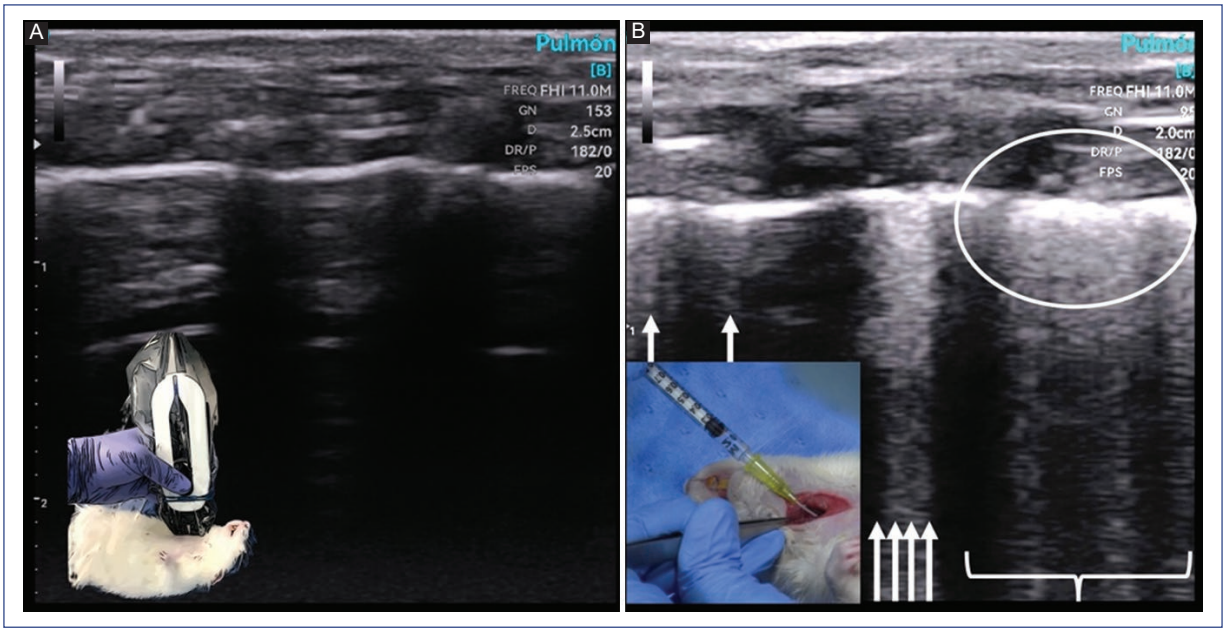

Figure 2. B-lines in an animal respiratory distress syndrome model. Bio model for teaching, respiratory distress syndrome. **A:** initial model showing pleural sliding, A-lines, and with M-mode, the seashore sign. **B:** after performing bronchoalveolar lavage with normal saline, surfactant is washed out, generating a thick and irregular pleural line (circle) and B-lines (arrows). B-lines appear colliding at the base giving the appearance of white lung (bracket: generalized alveolar-interstitial pattern with no spared areas).

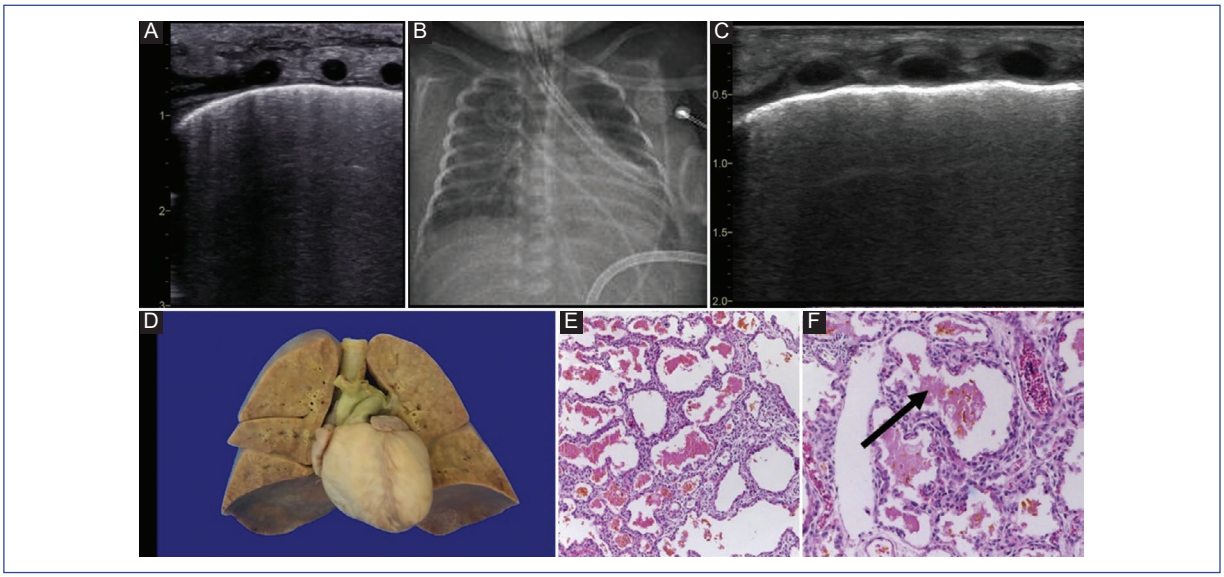

Figure 3. Acute respiratory distress syndrome (surfactant deficiency). Pre-term male infant born at 27 weeks of gestation from a dichorionic diamniotic twin pregnancy. Vaginal birth weighting 890g, twin A, intubated at birth receiving one dose of surfactant, transferred to tertiary level care. Birth-related injuries. Assessment for a second dose showed a lung ultrasound score (LUS) of 9, not predictive of re-surfactant administration. Developed early onset sepsis, transitional hypotension, acute renal failure, and intraventricular hemorrhage. **A** and **C:** lung ultrasound showing thick pleural line with coalescing B-Lines generating a white lung appearance, also described as alveolar–interstitial pattern with no spared areas (ground-glass sign). **B:** chest radiograph showing diffuse, bilateral, and symmetrical granular opacities (ground-glass appearance). **D:** lungs with homogeneous yellow consolidated parenchyma with small areas of hemorrhage. **E:** hematoxylin and Eosin (HE) ×100. Thickening of the interalveolar septa with a few lymphocytes is shown. Acellular eosinophilic material (hyaline membranes) with incipient hemorrhage is observed in the alveolar spaces. **F:** close up (×400) of alveolar space with formation of hyaline membranes (arrow).

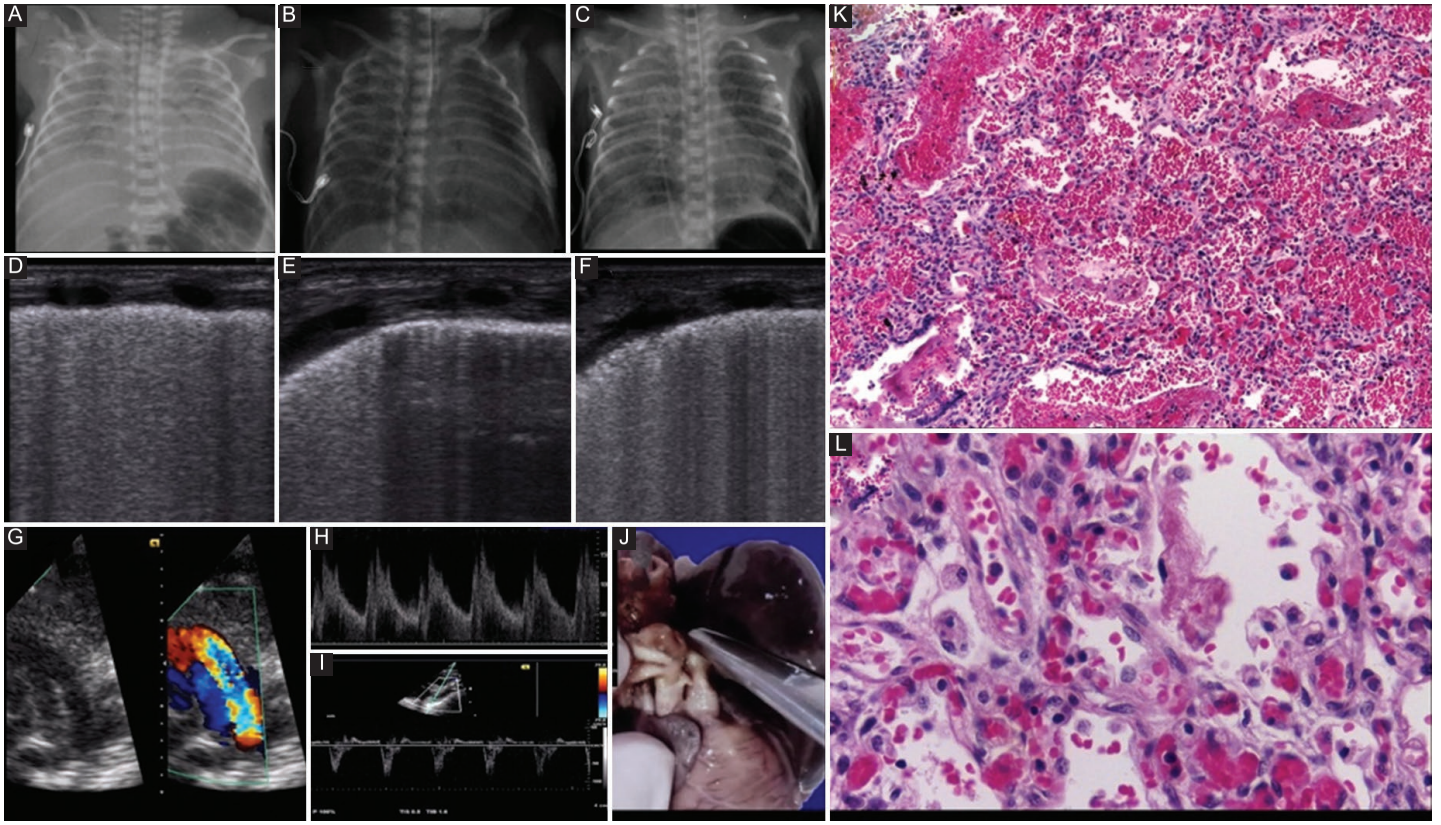

Figure 4. Respiratory distress syndrome, patent ductus arteriosus, and pulmonary hemorrhage. Pre-term male infant born at 28 weeks of gestation, weighting 820 g. Stabilized with continuous positive airway pressure (CPAP) after birth and transferred to a tertiary health facility. The first dose of surfactant was administered with a lung ultrasound score (LUS) of 14 with less invasive surfactant administration (LISA) technique that failed. After intubation, a second dose of surfactant with LUS of 12 was administered without adequate response. The echocardiogram showed a 2.8 mm hemodynamically significant patent ductus arteriosus (PDA). Pharmacological treatment with acetaminophen was attempted. Hypoxemic respiratory insufficiency developed, managed with high-frequency oscillatory ventilation (HFOV). Massive pulmonary hemorrhage developed. **A:** initial chest radiograph (CXR) with diffuse, bilateral granular opacities (ground-glass appearance). **B:** improvement after two doses of surfactant. **C:** pulmonary hemorrhage with CXR showing worsening of granular opacities with right predominance. **D:** lung ultrasound showing thick pleural line with coalescing B-lines generating a white lung appearance. **E:** after surfactant administration, areas with an interstitial B-line pattern, alternating with better aerated areas, were seen. **F:** before clinical massive lung hemorrhage, a thick irregular pleural line with static bronchogram was seen. **G:** a 2.8 mm left-to-right PDA is shown. **H:** pulsatile pattern on Doppler interrogation. **I:** reversed diastole in descending aorta. **J:** a large PDA was shown in the autopsy specimen. **K:** HE × 100. Alveolar collapse and extensive intra-alveolar hemorrhage. **L:** HE × 400. Focal hyaline membrane formation is seen.

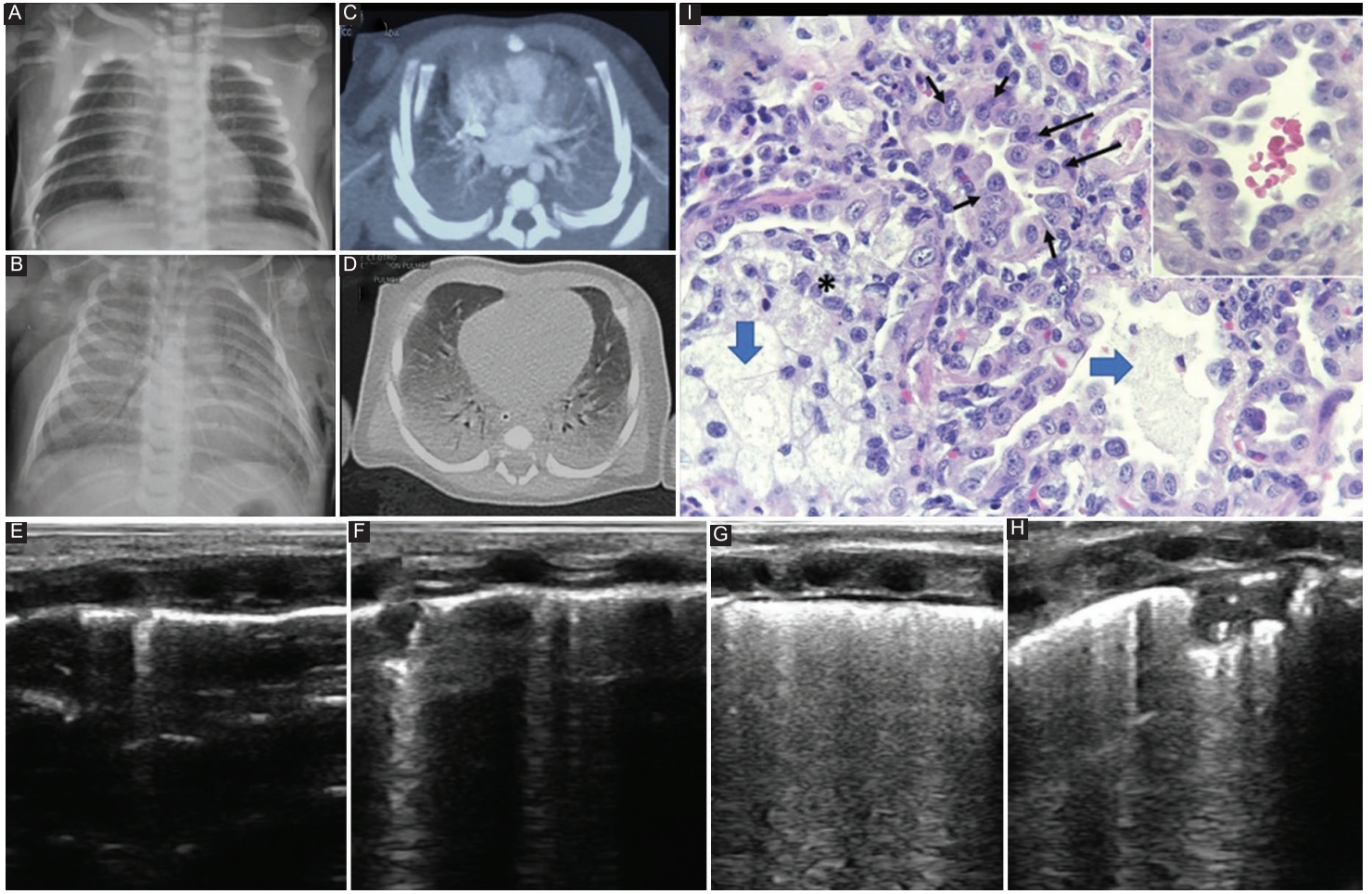

Figure 5. Congenital surfactant protein B (SP-B) deficiency. Late pre-term female born at 36.4 weeks of gestation. Routine resuscitation. Progressive tachypnea, increase in oxygen and CPAP requirements. **A** and **B:** chest radiograph showed progression to ground glass appearance. **C:** no significant pulmonary hypertension was found on echocardiogram, and vascular malformations were ruled out on contrast computed tomography. **D:** high-resolution computed tomography (HRCT) of the lung sowed diffuse ground glass pulmonary opacification consistent with early onset interstitial lung disease (ILD). **E** and **F:** progressive interstitial B-line pattern. **G:** progression to coalescing B-lines. **H:** progression to consolidations. A study protocol for ILD was performed without etiology, so a lung biopsy was performed on day 44, depicting histology consistent with SP-B deficiency. **I:** HE x 400. Hyperplasia and prominence of Type 2 pneumocytes completely surrounding the alveolar wall (black arrows), alveolar spaces filled with proteinaceous basophilic material (blue arrow), and abundant macrophages with microvacuole cytoplasm (*). Upper box with magnification of alveoli with prominent hyperplastic pneumocytes with a “tack” appearance, characteristic of surfactant deficiency.

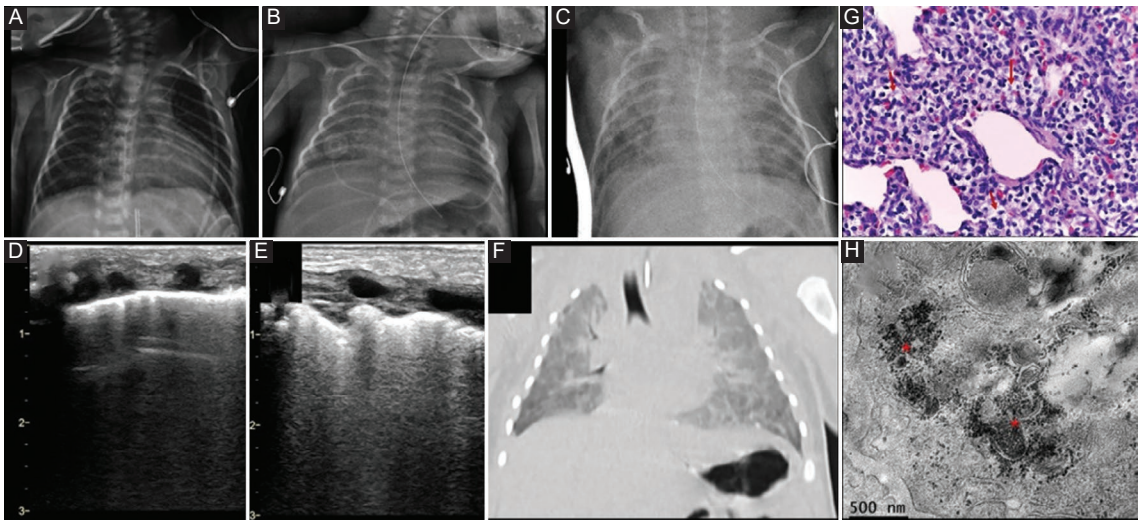

Figure 6. Pulmonary interstitial glycogenosis. Late pre-term female born at 34 weeks of gestation in a vaginal accidental delivery. The patient was stabilized in a private clinic and transferred to a tertiary care unit. Mild-to-moderate pulmonary hypertension was present. The patient was dependent on oxygen and CPAP. **A-C:** chest radiograph showed progressive granular opacities. **D** and **E:** lung ultrasound showed a progressive interstitial B-line pattern until coalescing B lines were present. **F:** HRCT consistent with early onset ILD. A lung biopsy was performed on day 47 showing: **G:** partial loss of architecture due to expansion of the interstitium at the expense of medium-sized cells with ample, clear cytoplasm and round to oval central nuclei. Periodic acid–Schiff staining reveals that these cells contain granular material in their cytoplasm that is digested by diastase, corresponding to glycogen. Histological section shows the thickening of the interalveolar septa due to the presence of cells with clear cytoplasm (arrows) and a scant lymphocytic infiltrate. **H:** ultrasonic photomicrograph with clusters of monoparticulate glycogen (*). Pulmonary Interstitial Glycogenosis was diagnosed. Treatment with steroids and diuretics commenced, and the patient was monitored in an outpatient clinic.

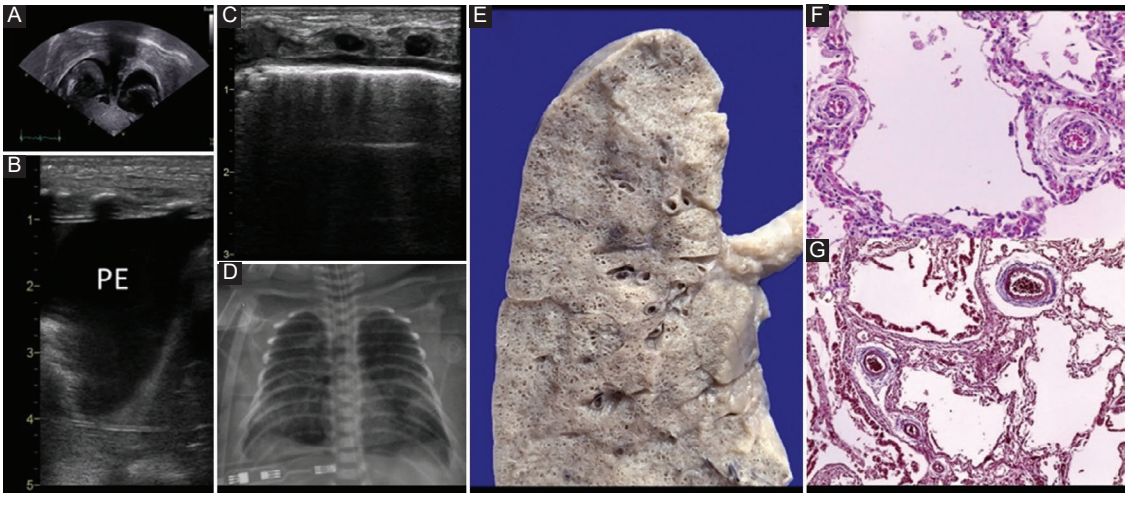

Figure 7. Pulmonary interstitial emphysema. Late pre-term male infant born at 34 weeks of gestation. Cesarean section secondary to premature rupture of membranes. Down syndrome with duodenal atresia. During Kimura duodenal-duodenal anastomosis, spontaneous hepatic rupture occurred. Acute renal failure and anasarca; renal replacement with peritoneal dialysis. Ventilated since birth, requiring high parameter and HFOV. Pleural effusion (PE) requiring needle drainage. **A:** transdiaphragmatic view showing bilateral PE. **B:** transversal view depicting a pool of 2 cm where 25 ml of transudate was evacuated. **C:** lung ultrasound taken hours before demise at 19 days of life showing a thick pleural line with a light B-line pattern, A-lines are also observed; a gap between the pleural line and chest wall is observed secondary to edema. **D:** chest radiograph showing soft-tissue edema and lung parenchyma with ten intercostal spaces and an interstitial pattern with opacities in both bases. **E:** pulmonary interstitial emphysema was diagnosed during autopsy. **F** (HE) and **G** (Masson's trichrome) ×100: alveolar spaces visibly dilated, with mild fibrosis of the interalveolar walls. There is concentric fibrosis of the adventitia of medium-caliber vessels.

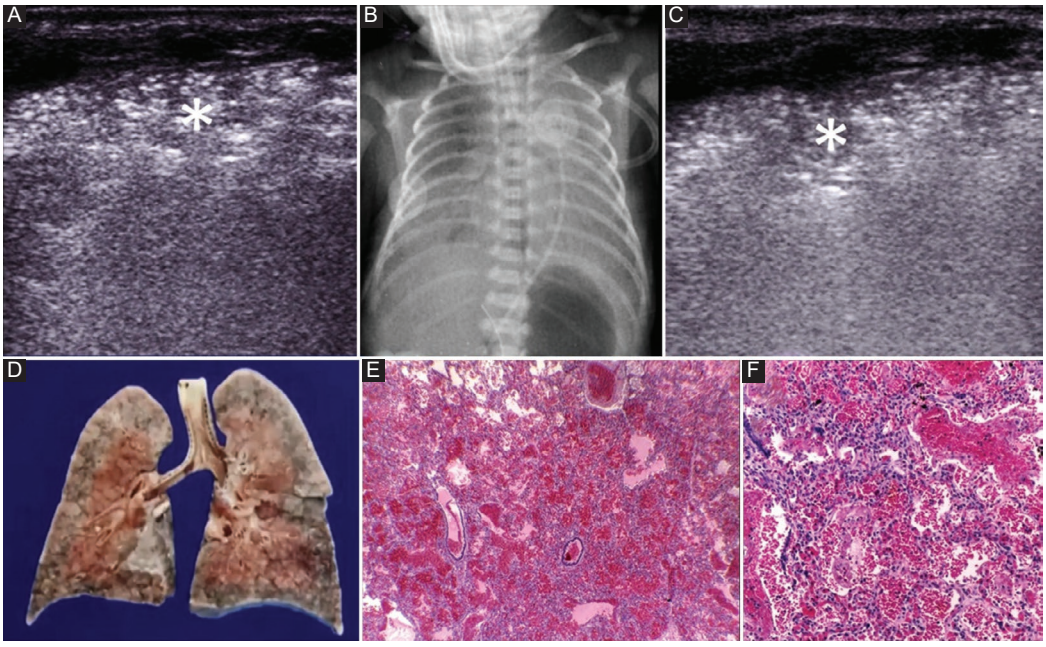

Figure 8. Early pulmonary hemorrhage. Pre-term male infant born at 28 weeks of gestation. Vaginal birth weighting 985 g. Intubated at birth receiving one dose of surfactant and transferred to tertiary level care. Assessment for a second dose showed a lung ultrasound score of 8, not predictive of re-surfactant administration. Early onset neonatal sepsis with septic shock and pulmonary hemorrhage. **A** and **C:** lung ultrasound showing shred sign, with consolidation and static bronchogram (*). **B:** chest radiograph showing granular opacities at the base of the right lung and across the left lung. **D:** lungs with consolidated parenchyma and extensive areas of hemorrhage **E:** HE ×100. Extensive intra-alveolar hemorrhage. **F:** HE ×400. Alveoli occupied by numerous erythrocytes; no inflammatory cells are observed.

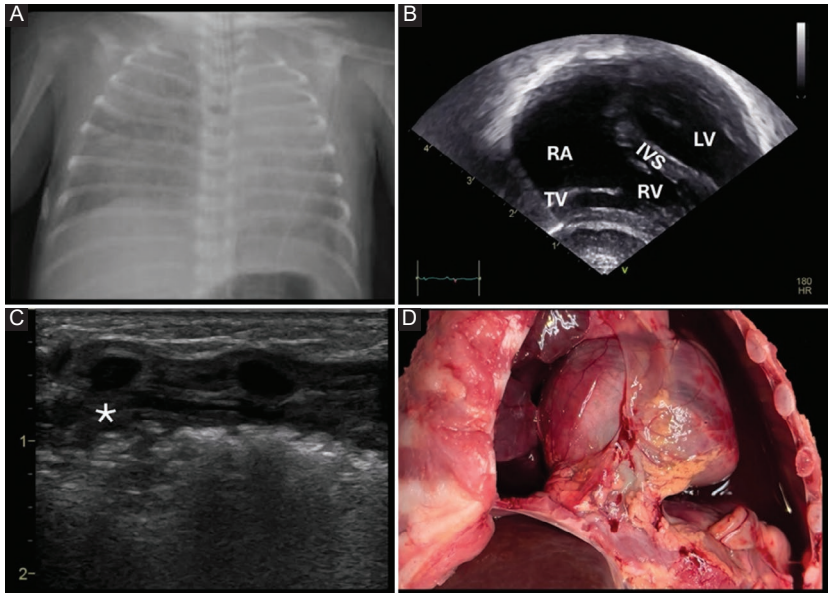

Figure 9. Congenital diaphragmatic hernia with late pulmonary hemorrhage. Severe left diaphragmatic hernia diagnosed at 26 weeks with an expected/observed lung to head ratio of 24%. Cesarean section at 37 weeks, 2730 g, female, intubated at birth. Hernioplasty performed on day 5. Developed severe pulmonary venous hypertension with left-to-right shunt through the patent foramen ovale, right atrial enlargement, and pulmonary hemorrhage. **A:** chest radiograph showing bilateral diffuse infiltrates with ground-glass opacities with a white out appearance. **B:** lung ultrasound with shred sign, with consolidation and fluid, and static bronchogram; fibrin deposition is shown (*). **C:** subcostal 4-chamber view depicting right atrium enlargement. **D:** autopsy specimen showing right atrial enlargement, with pulmonary hemorrhage and blood in the pleural space. RA: right atrium; TV: tricuspid valve; RV: right ventricle; IVS: interventricular septum; LV: left ventricle.

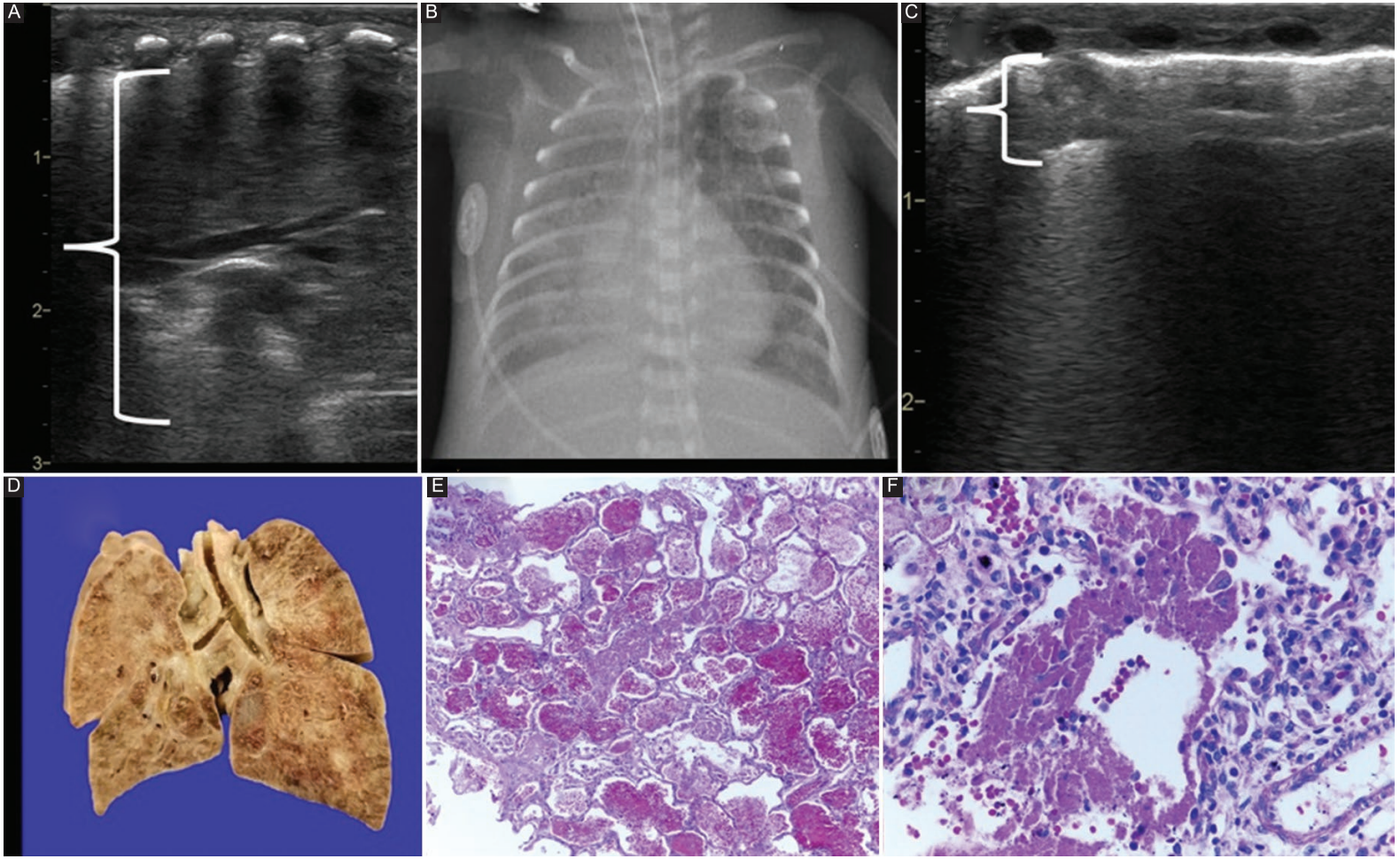

Figure 10. *Escherichia coli* hospital-acquired pneumonia. Pre-term male infant with intrauterine growth restriction born at 29 weeks' gestation by cesarean section weighting 690 g. Initially stabilized with CPAP without surfactant administration. Transferred to tertiary level care. Hemodynamically significant patent ductus arteriosus with pharmacological treatment. Healthcare-associated sepsis and septic shock with isolation of *E. coli*. Acute renal failure and fluid and electrolyte imbalance. **A** and **C:** lung ultrasound showing shred sign with extensive (**A**) and small (**C**) consolidations (bracket) with static and fluid bronchogram, alternating with areas with an alveolar–interstitial syndrome. **B:** chest radiograph showing diffuse opacification of the lung parenchyma with right predominance. **D:** lungs with heterogeneous consolidated parenchyma with areas of hemorrhage. **E:** HE ×100. Extensive intra-alveolar hemorrhage. **F:** HE ×400. Intra-alveolar hemorrhage and the formation of acellular eosinophilic necrotic material are seen.

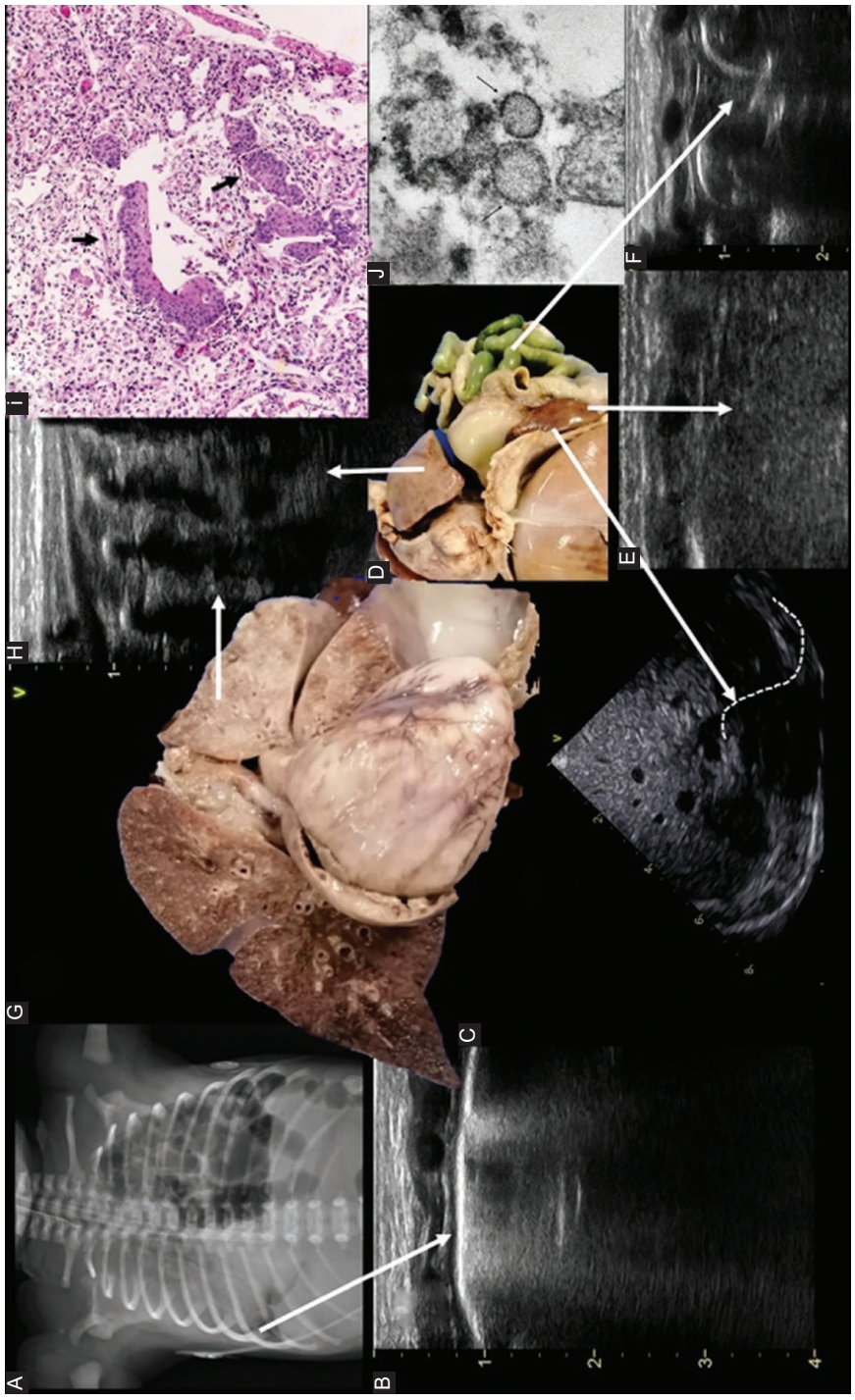

Figure 11. Congenital diaphragmatic hernia, perinatal asphyxia, and SARS-CoV-2 pneumonia. Severe left congenital diaphragmatic hernia (CDH) born during the first wave of the SARS-CoV-2 pandemic. Infant of a substance-abusing mother (cocaine/derivatives) born by an urgent cesarean section secondary to fetal tachycardia. Female weighting 3200 g. Intubated at birth. Perinatal asphyxia, transferred to a tertiary care center. HFOV with high oxygen requirements. During the 1st day of life, systemic hemorrhage occurred with a D-dimer of 60957 ng/ml. Real-time polymerase chain reaction positive to SARS-CoV-2. **A** and **B:** chest radiograph and lung ultrasound (LU) showing recruitment of the right lung during HFOV showing an interstitial B-line pattern, recommending no further increase in mean airway pressure. **C:** Transverse scan of the abdomen with partial absence of the hyperechoic line representing the normal diaphragmatic outline (dashed line). **D:** autopsy specimen showing severe CDH showing intestines and abdominal organs that can be seen in ultrasound as: **E:** presence of parenchymatous organs inside the thorax and **F:** absence of the hyperechoic line that represents the pleura and the absence of the normal A- lines in the affected hemithorax with multi-layered images with hyperechoic contents (intestine). **G:** cardiopulmonary block shows hypoplastic and consolidated left lung. **H:** posterior left longitudinal LU showing the consolidation. **I:** HE ×100. Squamous metaplasia is observed in some terminal bronchioles and alveoli (arrows); this change is described in COVID-19 infections. **J:** SARS-CoV-2 particles were seen by electron microscopy (arrows).

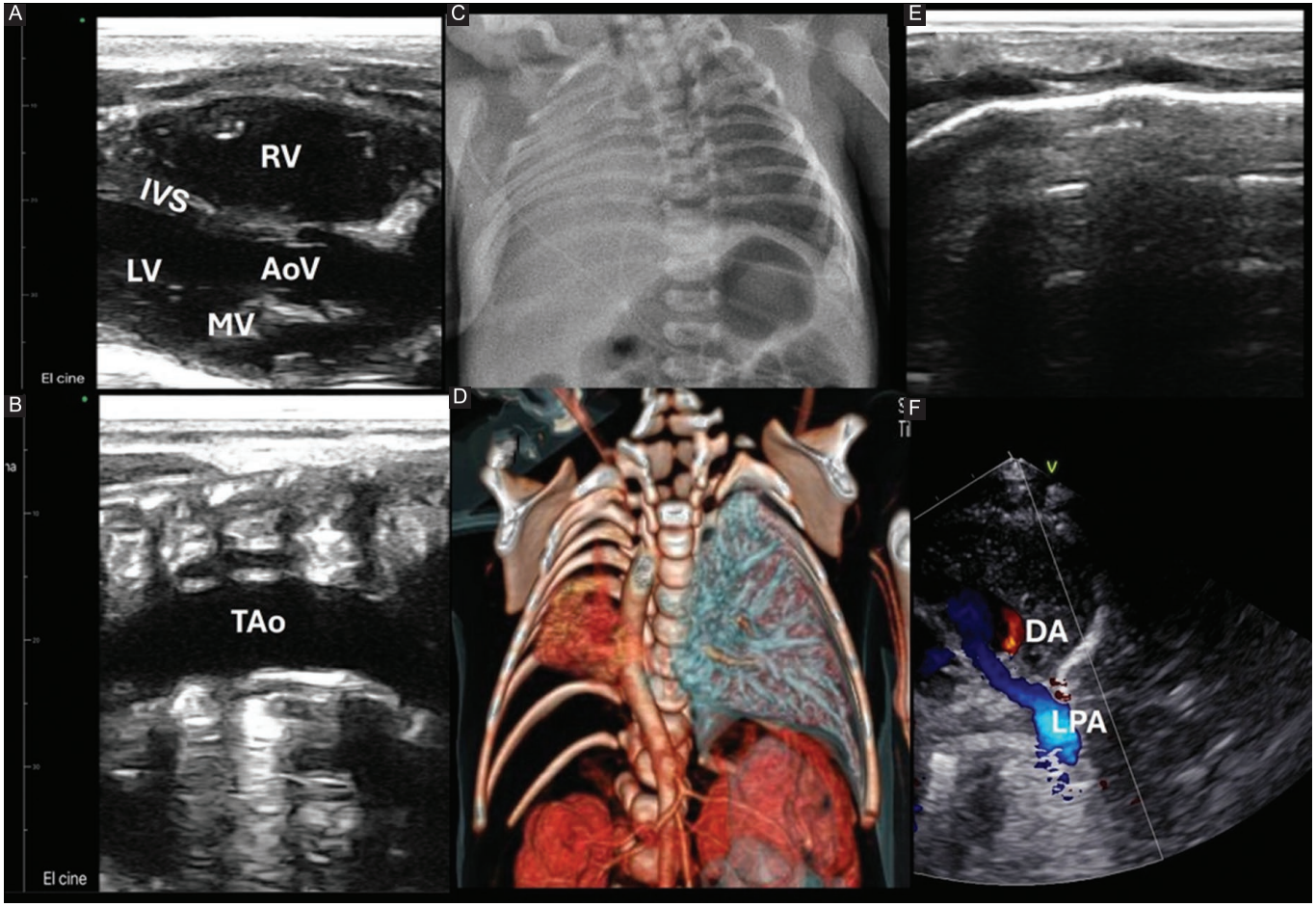

Figure 12. Right lung agenesis and VACTERL association. Term male infant born at 40 weeks of gestation. Urgent cesarean section secondary to fetal bradycardia weighting 2360 g. Low weight for gestational age. Without prenatal diagnosis, Type 3 esophageal atresia, anorectal malformation with rectoperineal fistula were diagnosed (VACTERL association). **C:** at arrival radiopacity of the right hemithorax is seen in chest radiograph. A lung ultrasound (LU) was performed to make differential diagnosis. **A:** on the right anterior thorax, the heart was found instead of lung artifacts (long axis view). **B:** posterior thorax where the thoracic aorta was identified with absence of the pleural line and any lung artifact or consolidation. **E:** LU of the left lung with normal appearance with pleural sliding and an A pattern. **D:** tomographic reconstruction confirming right lung agenesis with bronchi and pulmonary vessels absent. **F:** echocardiography showing absence of the right pulmonary artery (and pulmonary veins) with only the left pulmonary artery and the ductus arteriosus identified; a large atrial septal defect was also present. RV: right ventricle; IVS: interventricular septum; LV: left ventricle; AoV: aortic valve; MV: mitral valve; DA: ductus arteriosus; LPA: left pulmonary artery; TAo: thoracic aorta.

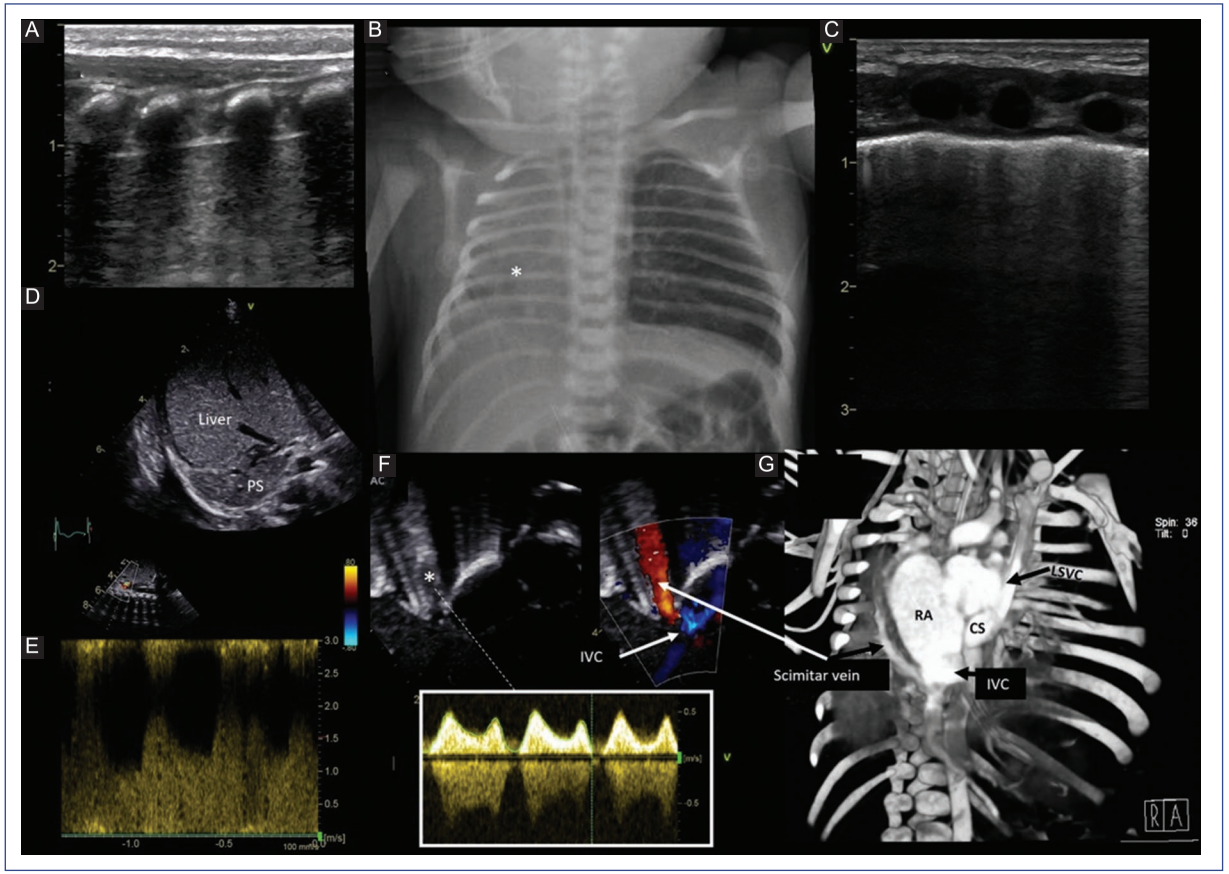

Figure 13. Right lung hypoplasia, intrapleural pulmonary sequestration, Scimitar syndrome, and VACTERL association. Term male infant born at 38 weeks of gestation. Cesarean section weighting 2885 g. Without prenatal diagnosis, referred to tertiary level care secondary to anorectal malformation, vertebral anomalies (VACTERL association), and dextroposition of the heart on the chest radiography. Sigmoidostomy was performed at arrival. **A:** lung ultrasound (LU) showing atelectatic lung on posterior fields only (on the right anterior and lateral thorax the heart was found) **B:** chest radiograph, note the crescent-shaped shadow [Turkish scimitar (asterisk)] in the right lower lung field (right pulmonary vein as it courses to join the inferior vena cava at the diaphragm [IVC]). **C:** LU showing interstitial B-line pattern. **D:** on the right lower lobe, an echogenic lesion was noted without cystic changes. **E:** blood supply from the aorta under the celiac trunk was documented, diagnosing bronchopulmonary sequestration (PS). **F:** echocardiography showed partial anomalous pulmonary venous return (PAPVR), note the of the infracardiac pulmonary vein (Scimitar vein) joining the IVC (cavoatrial junction), pulsed doppler with venous flow pattern of the Scimitar vein (lower box). Hypoplasia of the right pulmonary artery was documented. **G:** angiotomography documenting Scimitar syndrome: PAPVR of the infracardiac pulmonary veins to the inferior cavoatrial junction, diffuse hypoplasia of the right pulmonary branch, aberrant right subclavian vein, persistent left superior vena cava draining to the coronary sinus. Pulmonary sequestration of the lateral segment of the right lower lobe was found. RA: right atrium.

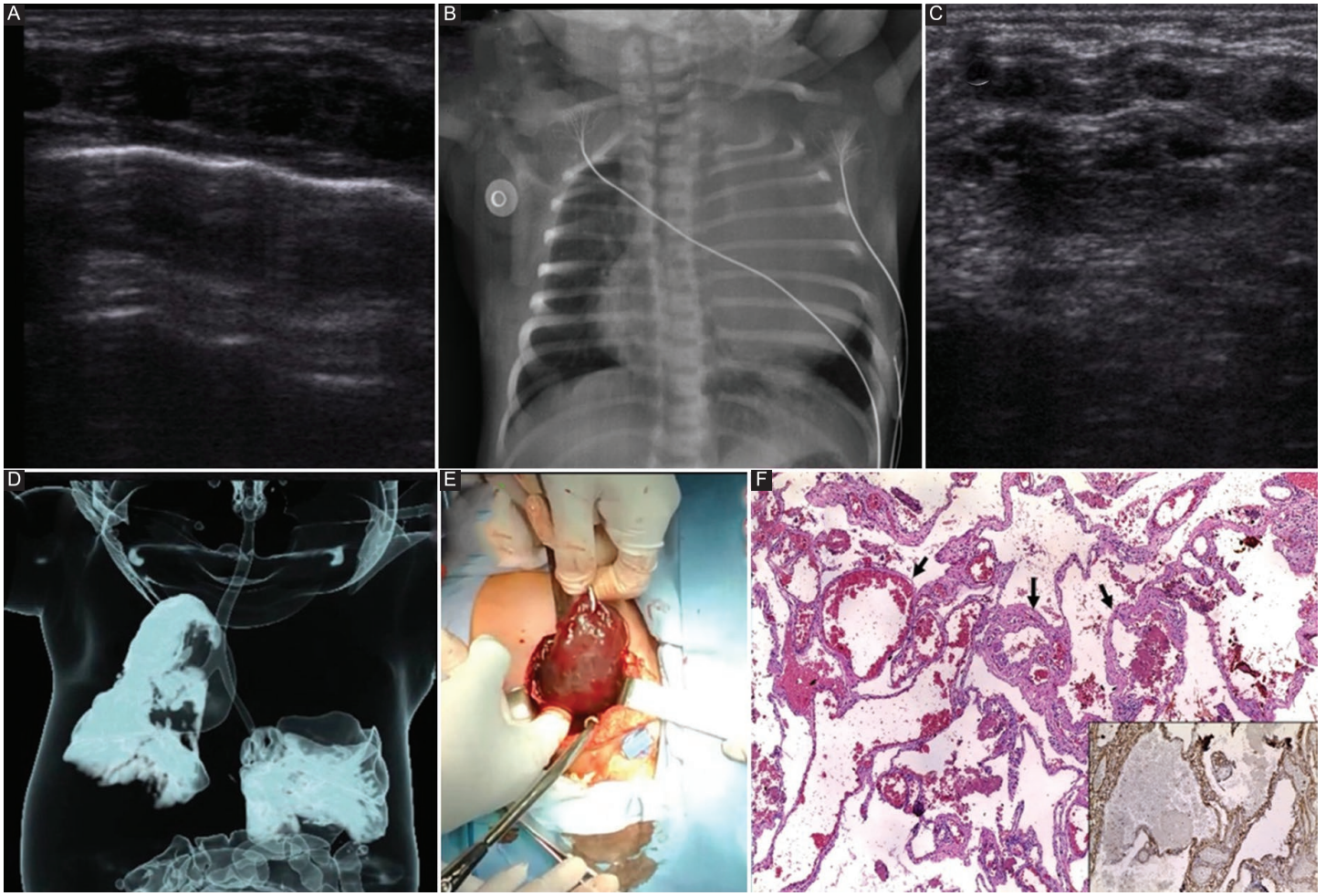

Figure 14. Pulmonary cavernous hemangioma. Term female infant born at 40 weeks of gestation. Vaginal delivery weighting 3070 g. Transferred to a tertiary care hospital secondary to a thoracic mass seen on chest radiograph (CXR) at birth (without prenatal diagnosis) **A:** lung ultrasound showing a normal right lung with pleural sliding and an A pattern. **B:** CXR showing a radiolucent, solid image on the left lung. **C:** lung malformation on the left lung, showing an irregular tissue-like pattern with multiple hypoechoic cystic images. **D:** tomographic reconstruction showing the normal lung parenchyma. **E:** surgical specimen. **F:** HE ×100. A lesion consisting of a proliferation of irregular thin-walled blood vessels (arrow) alternating between the alveolar spaces is observed (cavernous hemangioma). On the right box, immunohistochemistry for CD34 is observed, which is expressed in endothelial cells and vessel walls (brown chromogen).

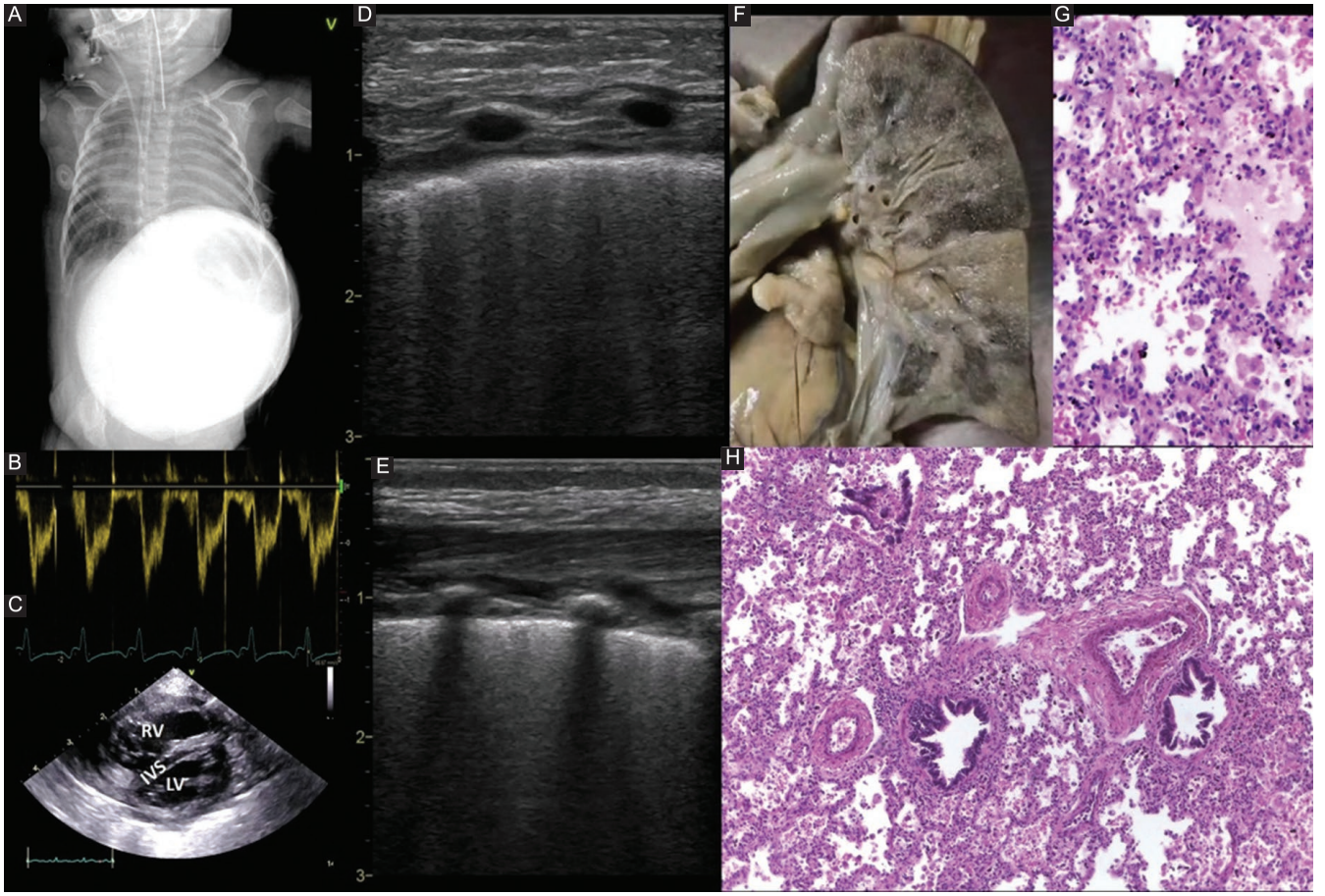

Figure 15. Bronchopulmonary dysplasia with pulmonary hypertension. Late pre-term female infant born at 35 weeks of gestation. Vaginal birth, intubated after not responding to three cycles of positive pressure ventilation. Omphalocele and left diaphragmatic hernia. Hernioplasty performed on day 15. Thirty-eight days ventilated mostly with HFOV. Multiple sepsis episodes developing neonatal acute respiratory distress syndrome. Under palliative care. **A:** chest radiograph showing intubation, cardiomegaly, and omphalocele. **B:** Pulsed Doppler of pulmonary artery revealing shortening of pulmonary artery acceleration time and mid-systolic notching consistent with pulmonary hypertension. **C:** short axis depicting a dilated right ventricle and flat to paradoxical intraventricular septum in systole. **D:** anterior lung ultrasound (LU) showing a thickened pleural line and a B-line interstitial heterogeneous pattern **E:** posterior LU showing a thickened pleural line and alveolar interstitial pattern. **F:** lung parenchyma with edema, consolidations, and hemorrhage **G**. HE ×400. Alveoli are shown with eosinophilic necrotic material, desquamation of pneumocytes, and the presence of alveolar macrophages. **H:** HE × 100. Parenchyma with desquamation of pneumocytes, intra-alveolar macrophages, and proliferation of concentric connective tissue in the adventitia of medium-sized vessels.

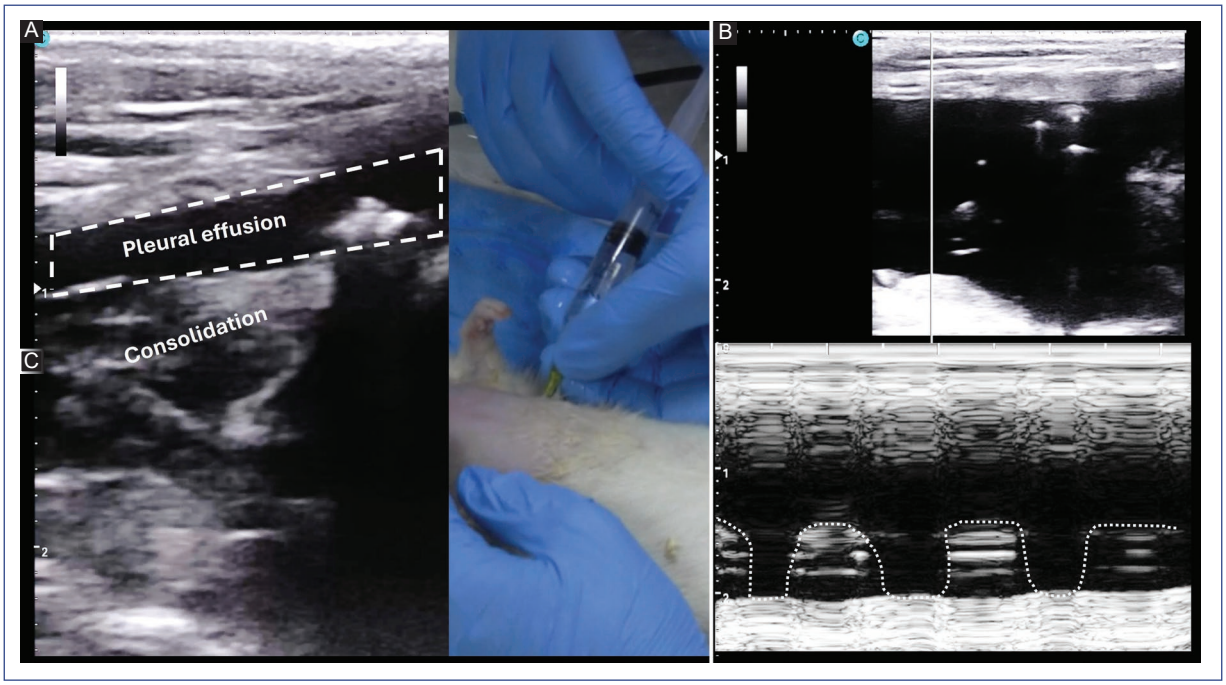

Figure 16. Animal model of pleural effusion (PE). Bio model for teaching, PE: **A:** after injecting 20 mL of normal saline into the pleural space, the 4-wall sign is identified (dashed square); note the consolidated lung (C) under it. **B:** on M-mode sinusoidal sign is identified (dotted line).

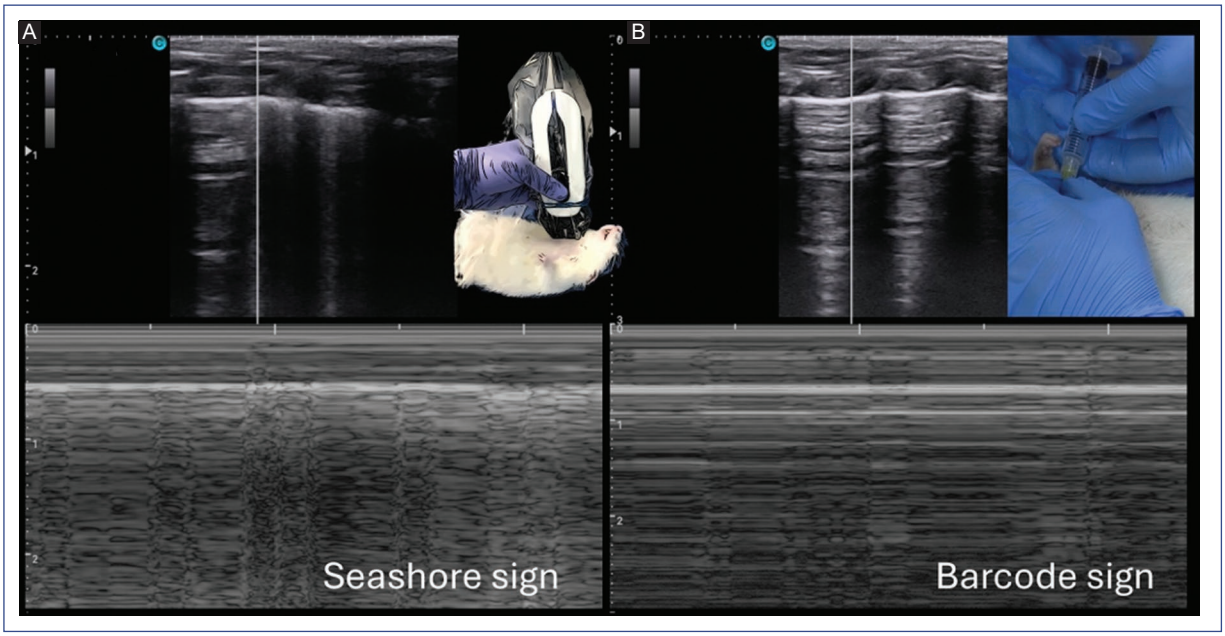

Figure 17. Animal model of pneumothorax. Bio model for teaching, pneumothorax: **A:** initial model showing pleural sliding, A-lines alternating with B-lines, and with M-mode the seashore sign. **B:** after injecting 15 mL of air into the pleural space, pleural sliding and B-lines disappear, only A lines are visible, and in M-mode, the barcode sign is depicted.

evolving and chronic lung disease, defined as bronchopulmonary dysplasia (BPD)[4] and increased pulmonary blood flow (example, patent ductus arteriosus, Fig. 4), and coalescent B-lines can be seen in neonatal acute RDS (NARDS)[5]. Persistent tachypnea and an increasingly progressive B-line pattern can help to identify early onset interstitial lung disease (Figs. 5 and 6)[6]. One of the limitations of LU is its inability to diagnose overdistension, so caution is recommended, as B-lines can be seen even in an overdistended lung (Fig. 7).

Consolidation

A consolidation is a subpleural hypoechoic region with shredding of the pleural line, with tissue-like echotexture and disappearance of A-lines. Static or dynamic air bronchogram can be found. Consolidations are seen in meconium aspiration syndrome, pulmonary hemorrhage (Figs. 8 and 9), atelectasis, pneumonia (viral, bacterial, fungal [Figs. 10 and 11]), NARDS, and BPD[7,8].

Lung malformations

LU has been used to confirm or suspect lung and airway malformations by identifying absence of normal lung parenchyma artifacts and hypoechoic micro- or macro-cystic images, multiple hypoechoic irregular patterns, and consolidations. A displaced heart can be found in cases of atelectasis, congenital diaphragmatic hernia, and pulmonary hypoplasia/agenesis. It is always necessary to complement its study with high-resolution lung computed tomography and angio tomography (Figs. 11-14)[9-12].

Chronic lung disease

BPD is characterized by a thickened pleural line, B-line interstitial heterogeneous pattern, and consolidations. Integrated LU and targeted neonatal echocardiography assessment enhances the delineation of different phenotypes, disease monitoring, and individualized guidance physiology-based management (Fig. 15)[4,13].

Pleural effusion (PE) and pneumothorax (PTX)

LU is the gold standard to diagnose PE and PTX. "Crashing infant" ultrasound protocols have been described for prompt diagnosis and treatment[14,15].

PE

It is recognized by a missing bat sign and identifying the four walls sign, and an anechoic area that separates the parietal pleura from the visceral pleura and compresses the lung. In M-mode, with each respiratory cycle, the lung surface line will move toward the pleural line creating a sinusoidal sign (Fig. 16).

PTX

To diagnose, it is necessary to note absent pleural sliding and only A-lines (one B-line rules out the possibility). There should be no "pulmonary pulse," that is, the absence of pleural sliding and clear visualization of cardiac pulsations at the level of the pleural line, as this sign may reflect main stem intubation of the contralateral lung. The presence of a lung point, which is the point that separates sliding from a non-sliding area, is a specific sign of a PTX (mild-moderate), but its absence does not exclude it as it is the case in tension PTX. On M-mode, the barcode sign generated by the absence of pleural sliding losing the sandy appearance, and a series of horizontal parallel lines are seen (Fig. 17).

Conclusion

Animal models and clinical cases with tomographic reconstructions, biopsies, or autopsies were presented showing the basic semiology and the usefulness of LU to diagnose and monitor neonatal respiratory diseases.

Acknowledgments

The authors would like to thank Dr. Stanislaw-Sadowinski Pine and Dr. Ma. de L. Cabrera-Muñoz for their support in reviewing pathological anatomy cases for the neonatal pulmonary ultrasound program at the Federico Gómez Children's Hospital of Mexico from 2017 to 2023. We also thank Dr. Irma A. Coronado-Zarco and Dr. Jorge A. Cardona-Pérez for their support of the bedside ultrasound program at the Isidro Espinoza de los Reyes National Institute of Perinatology (2023-2024).

Funding

The authors declare that they have not received funding.

Conflicts of interest

The authors declare no conflicts of interest.

Ethical considerations

Protection of humans and animals. The authors declare that the procedures followed complied with the ethical standards of the responsible human experimentation committee and adhered to the World Medical Association and the Declaration of Helsinki. The procedures were approved by the Institutional Ethics Committee.

Confidentiality, informed consent, and ethical approval. The authors have obtained approval from the Ethics Committee for the analysis of routinely obtained and anonymized clinical data, so informed consent was not necessary. Relevant guidelines were followed.

Declaration on the use of artificial intelligence. The authors declare that no generative artificial intelligence was used in the writing of this manuscript.

References

1. Ibarra Ríos D, Sánchez-Cruz A. Ultrasonido pulmonar en neonatología. In: Programa de Actualización Continua en Neonatología-5/Libro 6, PAC®. Mexico: Intersistemas S.A. De C.V; 2021.
2. Piskovská A, Kraszewska K, Hauptman K, Jekl V. The rat thoracic ultrasound protocol: scanning technique and normal findings. Front Vet Sci. 2024;11:1286614.
3. Raimondi F, Yousef N, Migliaro F, Capasso L, De Luca D. Point-of-care lung ultrasound in neonatology: classification into descriptive and functional applications. Pediatr Res. 2018;90:524-31.
4. Sánchez-Becerra JC, Guillén-Torres R, Becerra-Becerra R, Márquez-González H, Ibarra-Ríos D. Targeted neonatal echocardiography and lung ultrasound in preterm infants with chronic lung disease with and without pulmonary hypertension, screened using a standardized algorithm. Front Pediatr. 2023;11:1104940.
5. De Luca D, Van Kaam AH, Tingay DG, Courtney SE, Danhaive O, Carnielli VP, et al. The montreux definition of neonatal ARDS: biological and clinical background behind the description of a new entity. Lancet Respir Med. 2017;5:657-66.
6. Marczak H, Krenke K, Griese M, Carlens J, Seidl E, Gilbert C, et al. An update on diagnosis and treatments of childhood interstitial lung diseases. Breathe (Sheff). 2025;21:250004.
7. De Luca D, Foti A, Alonso-Ojembarrena A, Condò V, Capasso L, Raschetti R, et al. Lung consolidation depth and gas exchange in different types of neonatal respiratory failure. Chest. 2024;165:1431-4.
8. Ibarra-Ríos D, Enríquez-Estrada AC, Serpa-Maldonado EV, Miranda-Vega AL, Villanueva-García D, Vázquez-Solano EP, et al. Lung ultrasound characteristics in neonates with positive real time polymerase chain reaction for SARS-CoV-2 on a tertiary level referral hospital in Mexico City. Front Pediatr. 2022;10:859092.
9. Yousef N, Mokhtari M, Durand P, Raimondi F, Migliaro F, Letourneau A, et al. Lung ultrasound findings in congenital pulmonary airway malformation. Am J Perinatol. 2018;35:1222-7.
10. Corsini I, Parri N, Coviello C, Leonardi V, Dani C. Lung ultrasound findings in congenital diaphragmatic hernia. Eur J Pediatr. 2019;178:491-5.
11. Weber J, Sati SK, Karody VR. Unilateral lung agenesis: a case series and review of literature. AJP Rep. 2023;13:e40-3.
12. Jaramillo González C, Karam Bechara J, Sáenz Gómez J, Siegert Olivares A, Jamaica Balderas L. Síndrome de la cimitarra: serie de casos. Bol Med Hosp Infant Mex. 2014;71:367-72.
13. Savoia M, Busolini E, Ibarra Ríos D, Thomas B, Ruoss JL, McNamara PJ. Integrated lung ultrasound and targeted neonatal echocardiography evaluation in infants born preterm. J Pediatr. 2024;275:114200.
14. Yousef N, Singh Y, De Luca D. "Playing it SAFE in the NICU" SAFE-R: a targeted diagnostic ultrasound protocol for the suddenly decompensating infant in the NICU. Eur J Pediatr. 2022;181:393-8.
15. Ibarra-Ríos D, Serpa-Maldonado EV, Mantilla-Uresti JG, Guillén-Torres R, Aguilar-Martínez N, Sánchez-Cruz A, et al. A modified sonographic algorithm for image acquisition in life-threatening emergencies in the critically Ill newborn. J Vis Exp. 2023;(194):1-24.